GEOPHYSICS

Global subduction slow slip events and associated earthquakes

Kélian Dascher-Cousineau[1,2]* and Roland Bürgmann[1]

Three decades of geodetic monitoring have established slow slip events (SSEs) as a common mode of fault slip, sometimes linked with earthquake swarms and in a few cases escalating to major seismic events. However, the connection between SSEs and earthquake hazard has been difficult to quantify and contextualize beyond regional studies. We aggregate a geodetic record of SSEs from subduction zones in the circum-Pacific region. In aggregate, earthquake rates increase up to threefold concurrent with and proximal to SSEs. The relative amplitude of this increase is correlated with the SSE size and, to a lesser extent, their depth and region. The subdued and coincident earthquake response to SSE stress transfer suggests a more limited role of static stress transfer and a very short relaxation timescale for the triggered seismicity. The observed range of behavior does not support a major connection between SSEs and earthquake hazard.

INTRODUCTION

High-resolution geodesy reveals that both earthquakes and slow slip can accommodate fault motion (*1*–*4*). A patchwork of slow- and fast-slipping regions transfers stored elastic energy in the lithosphere (*5*), and slip can be steady or episodic. The latter, slow slip events (SSEs), span days to years—often with an equivalent magnitude comparable to damaging earthquakes but without the associated shaking (*4*, *6*, *7*). The transience and large magnitude range of SSEs provides a unique opportunity to diagnose slow slip, stress transfer, and its relationship to earthquake nucleation (Fig. 1A).

Systematic study of SSEs has led to regional datasets and, alongside, hypotheses about how SSEs interact with earthquakes. These hypotheses range from SSEs altogether inhibiting earthquake occurrence (*8*) to SSEs representing the onset of the earthquake nucleation process (*9*–*17*). Earthquake rates leading up to, during, and following SSEs hold clues about the interplay of earthquakes and slow slip as outlined in Fig. 1B. With small SSE inventories, however, representative measures remain elusive. Some SSEs are associated with increased earthquake rates (*18*–*20*), and others are not (*21*). Whether this variability arises from the analytical approach, regional context, or local heterogeneity, and whether there are emergent signatures shared among the accompanying earthquake rates is still unclear.

We assemble a global catalog of geodetically detected SSEs for 10 well-monitored regions (*6*, *10*, *11*, *13*, *22*–*48*). After preprocessing and merging, the catalog comprises 923 unique SSE detections (Fig. 2). These SSEs are considered alongside global earthquake catalogs (*49*–*51*). We use this combined dataset to quantify the temporal and spatial relationship between slow slip and earthquake rates. We seek representative answers to the following questions: What are the temporal and spatial characteristics of earthquakes occurring alongside SSEs? How often are SSEs directly associated with large earthquakes or a transient increase in earthquake rates? How different is this interplay from one region to another? Documenting these facets provides a foundation to determine short-term earthquake hazard and the acting mechanisms for earthquake nucleation.

[1]Department of Earth and Planetary Science,University of California, Berkeley, Berkeley, CA, USA. [2]Miller Institute for Basic Science, Berkeley, CA, USA.
*Corresponding author. Email: kdascher@berkeley.edu

RESULTS

Temporal change in seismicity rate

We first document relative seismicity rates before, during, and after SSEs by stacking nearby earthquakes. Aggregating the observations increases the statistical power of the analysis and enhances generalizable patterns. See Materials and Methods for full documentation of the data preprocessing for the catalog.

For each SSE, we select all earthquakes with $M \geq 4.0$ within 50-km horizontal distance from the centroids of SSEs with a geodetic moment magnitude (M_w) ≥ 5.5, ±20 km of the slab interface, and ±7.5 source durations from the slow slip centroid time (table S3). For simplicity and legibility, we use fixed spatial windows. Scaling the search radius to the size of the SSEs has a negligible effect on the ensuing analysis (fig. S6), which focuses on the temporal evolution of the earthquake rate and is dominated by the small to moderate SSEs. Thus, each SSE has a corresponding space-time window that contains a set of earthquakes. A stack combines these windows. The timing of earthquakes in the stacks is relative to the corresponding centroid time of SSEs and normalized by the duration of the SSEs.

We present two stacks documenting the relative timing of earthquakes: a raw stack and a density stack. The former simply reports a stacked histogram of the relative timing of earthquakes (Fig. 3A). It exhibits higher earthquake rates in four distinct maxima, one preceding the occurrence of slow slip, one coincident, and two subsequent maxima. Four individual windows disproportionately contribute to the peaks not centered on the SSE centroid. Strong earthquake clustering largely accounts for this effect and is a common challenge for quantifying the effect of slow slip. Nonetheless, this raw stack not only hints at elevated rates of earthquakes during slow slip but also highlights just how variable the interplay can be.

The density stack quantifies temporal earthquake densities, relative to a constant rate, in each window of observation. The stack is conditional on there being any earthquake in the selected window of observation. Adding the temporal densities, which integrate to one for each window, largely removes the outsized effect of earthquake clusters. Thus, we forgo declustering of the earthquake catalog, avoiding the assumptions and limitations thereof. The density stack also introduces Gaussian kernels to account for uncertainty in timing of the SSEs relative to the earthquakes. This relative timing uncertainty is large, in some cases exceeding the duration of the event itself (*35*).

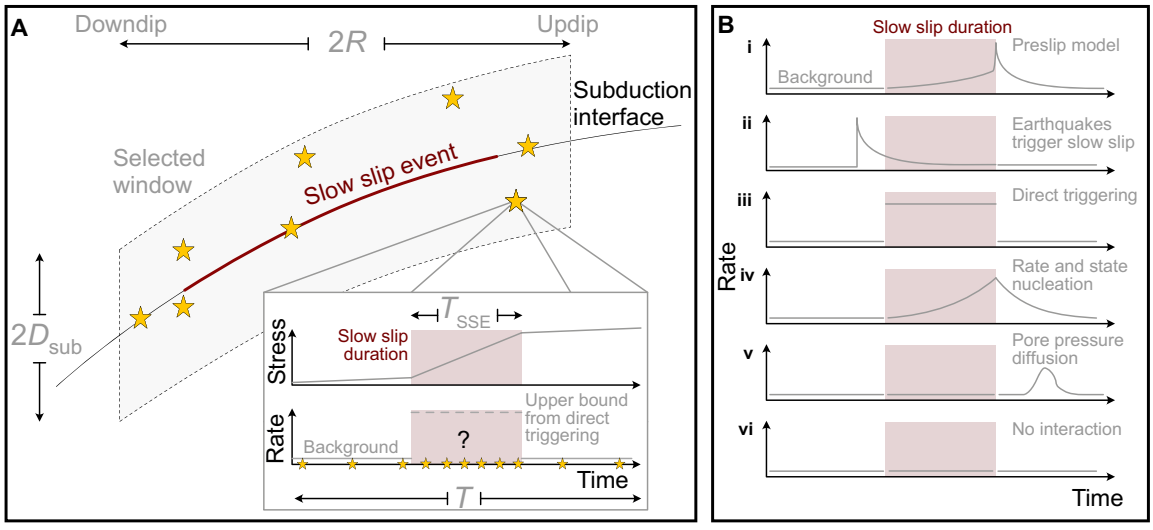

Fig. 1. Interplay between SSEs and earthquake nucleation. (**A**) Idealized cross section of subduction zone hosting an SSE. Slip transfers stress in surrounding volume, approximated here with a radius R and D_{sub} kilometer above and below the subduction zone interface. Stars are examples of potential nucleation sites in the upper plate, lower plate, and interface. Slow slip transiently increases the stressing rate (inset) over its duration T_{SSE}; how earthquake rates respond over the interval T is an open question. (**B**) Conceptual earthquake rate fingerprints for inferred earthquake-slow slip interplay. (i) The preslip model suggests that slow slip drives foreshock activity and culminates in the occurrence of a large earthquake (*15*, *16*, *54*, *83*). (ii) An earthquake triggering model, not to be confused with afterslip, which we do not explore here, suggests that the onset of slow slip is frequently the result of seismic waves passing by (*73*). (iii) A direct triggering model is often used or assumed in statistical treatments of earthquake swarms, wherein the earthquake rate increases with the moment rate (*19*, *20*, *57*, *58*, *67*, *84*, *85*). (iv) A rate and state nucleation model predicts a lag between the SSE occurrence and seismicity (*75*, *76*, *86*). The timescale dictating the lag is determined by the stress state and material properties; if it is larger than the duration of slow slip, as is typically assumed, then earthquake rates should be highest toward the end of the SSE. (v) The passage of fluids associated with slow slip would enable seemingly distinct timing for slow slip and earthquakes without a clear prediction for the relative timing (*19*, *86*–*89*). (vi) No interaction, as implied if the phenomena occur in frictional regimes that are sufficiently far from each other to be isolated (*21*).

For more detail and the complete justification of the approach refer to Materials and Methods, particularly Eq. 1.

The density stack indicates that earthquakes occur disproportionately during SSEs. To assess the statistical significance of the increased rate, we produce 10,000 new stacks, substituting the SSE centroid times with random times in the 1994 to 2021 interval in each iteration. These random stacks establish a background level and its variability. During the SSEs, the density stack is, on average, a factor of 1.24 ± 0.22 higher than the background level. The increase in seismicity is not predicated on any individual region (fig. S1A); all regions tend to have more earthquakes during SSEs than otherwise (fig. S1B). The exact amplitude depends on the windowing parameters and event magnitudes and so should not be taken as absolute but rather as an overall measure of increased seismicity in the vicinity of SSEs. There is a tradeoff between reduced statistical power and increased effect size when selecting larger SSEs or larger earthquake magnitudes. Higher cutoffs for the earthquake magnitude also result in more intense earthquake triggering (Fig. 3E), potentially reflecting a tendency for larger earthquakes during slow slip (fig. S2). Triggering is generally stronger near the centroid and asymptotically approaches the background with increasing distance (Fig. 3D). Lastly, considering larger SSEs tend to yield stronger signals (up to ~3-fold in Fig. 3F), scaling approximately as $[r/r_{back} - 1] \sim M_{min\text{-}SSE}^{0.4}$, where r/r_{back} is the earthquake rate relative to a steady background rate in the corresponding window (Fig. 3F and fig. S7).

Our first key finding is a statistically significant increase in seismicity concurrent with slow slip. The amplitude of this increase is small compared to seismicity (aftershocks) associated with earthquakes; as a point of reference, an increase on the order of 100 to 1000 is more typical for comparably sized earthquakes, even when only considering mainshocks nearly colocated with the SSEs featured in this study (fig. S9).

Spatial variation in seismicity

We next document how slow slip influences the seismicity's spatial structure. We stack earthquakes using the same density approach, now in two spatial dimensions (see Materials and Methods). Figure 4 shows the spatial distribution of earthquake epicenters before, during, and after slow slip (see also fig. S3 for the raw stack). We interpret the distribution of earthquakes before the onset of slow slip as reflecting structural characteristics of the collection of subduction zones (see also figs. S3 to S5). There is a slightly lower density of earthquakes in the zone with impending slow slip (Fig. 4A). During SSEs, this same zone features the highest level of contiguous earthquake density (Fig. 4B). The ratio in densities before and during SSEs, as shown in Fig. 4B, highlights this dichotomy. The stack features a relative increase in event density that reaches its maximum within the approximate footprint of the SSEs (Fig. 4C). Separating SSEs that are located up dip or down dip of the seismogenic zone highlights increased seismicity colocated with the SSE and, notably, in the seismogenic zone (figs. S4 and S5). Stacking, as in Fig. 4, averages out and potentially masks structural features shared only by a subset of the data. To summarize, our second key finding is a less than twofold increase in seismicity—still a maximum in the global spatial stack—within the footprint of the slipping area.

(Un)productive SSEs and regional variations

Of the 923 SSEs considered, ~400 had no $M \geq 4$ earthquakes in the space-time windows considered (fig. S8). The proportion strongly

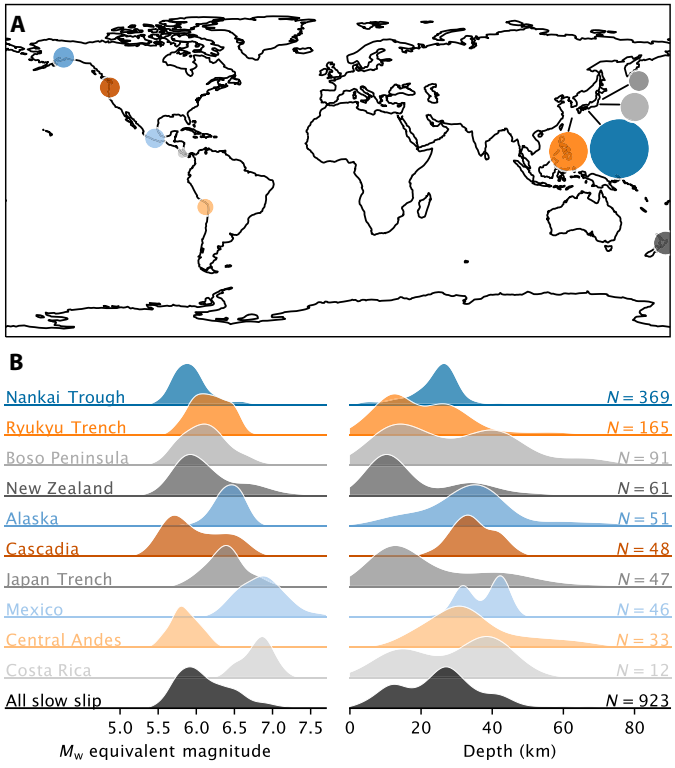

Fig. 2. A global dataset of SSEs. (**A**) Location of considered subduction zones. (**B**) Geodetic equivalent event moment magnitudes range from M_w 5 to 7.5 with clusters of events at 12, 28, and 45 km in depth (using K_d clustering with three clusters). Each region, however, seems to have a roughly bimodal depth distribution of SSEs. *N* refers to the number of unique SSE detections (see Materials and Methods).

depends on the selected parameters for the minimum earthquake and slow slip magnitude in the analysis. These events are disproportionately in Nankai and Cascadia, which feature many tremor-producing, deep-seated, and small-magnitude SSEs. The collection of particularly unproductive SSEs suggests that there are SSEs notable for their high earthquake productivity. We label an SSE as productive if colocated preceding windows rarely (<5%) exhibit as many earthquakes as occurred during the SSE (see Materials and Methods). This subset corresponds to the top 6% most productive SSEs in the dataset and disproportionately occurs in a subset of regions (Fig. 5A). The most productive regions are Costa Rica, Mexico, the Japan trench, and the Boso Peninsula; the least productive regions are Cascadia, Nankai, and Alaska. This ordering is subject to uncertainty. The bootstrap sampling of the collection of SSEs in this study illustrates this well. The subsamples of the data yield a large spread in the relative representation of more productive SSEs (Fig. 5A). Nonetheless, the relative scarcity of productive SSEs in Nankai and Cascadia is robust to the resampling.

More productive SSEs appear to be shallower and larger than the global set [$P = 0.05$ and 0.003, respectively, using a two-tailed Kolmogorov–Smirnov (KS) test; see also Fig. 5, B and C]. We estimate SSE moment rates as the equivalent moment divided by the duration. Even with this relatively large dataset, it is difficult to robustly assess the influence of the moment rate on the relative productivity of these SSEs (Fig. 5D).

It is generally difficult to disentangle causal relationships. Cascadia and Nankai tend to feature comparatively smaller, deeper, and tremor-producing SSEs. These factors perhaps confound regional differences or vice versa. Nonetheless, it appears meaningful to highlight that (un)productive events are samples from distinct subpopulations of SSEs. Anecdotally, within the Nankai dataset, shallower events tend to feature more earthquakes during SSEs (fig. S8). Our third key finding is that different tectonic settings feature persistent differences in how slow slip and earthquake relate.

DISCUSSION

The compilation of SSEs reveals an increase in earthquake abundance that is detectable and measurable in global stacks. The relative abundance of earthquakes is 1.24 ± 0.22 higher during SSEs (Fig. 3). If there is a lag in the onset of earthquakes, then it is shorter than the duration of the SSEs and the uncertainty in their timing. The amplitude of the rate increase scales with the slow slip moment (Fig. 3 and fig. S7). The rate almost monotonically increases for smaller spatial windows (Fig. 3D). Spatial stacks indicate that the increase in seismicity corresponds well with the estimated timing and location of the SSEs (Fig. 4). These measurements about the average amplitude, timing, and location as well as the substantial variability therein are key observables enabled by the global dataset with both hazard and mechanical implications.

Before discussing implications further, we underscore that stacking can obscure some aspects of the interplay between SSEs and earthquakes. Many (~40%) of the time intervals we consider have no earthquakes to establish rate changes. Relatedly, the analysis considers changes in rate as normalized with the corresponding background rate; thus, some of the productive SSEs in otherwise quiet environments have a small influence on the absolute count of earthquakes. Conversely, an SSE that propagates toward regions prone to very large earthquakes might cause alarm (*52*). Some recurring SSEs repeatedly accompany vigorous earthquake sequences, as has been documented for select events in the Boso Peninsula [e.g., (*18*)]. Similarly, the significant regional differences (Fig. 5) suggest that the interplay can be persistent in time for a given location.

Slow slip and earthquake hazard

A combination of laboratory, modeling, and observational evidence suggests that slow slip might enable the nucleation of large earthquakes in particular (*9*, *11*, *13*–*16*, *53*–*55*). Yet, our dataset underscores that SSEs without associated enhanced earthquake activity are very common, and, in this sense, SSEs that trigger large earthquakes are rare. We may still test whether there is a bias for large earthquakes to closely follow SSEs, perhaps indicating a causal relationship. Six of the 923 SSEs had an M6.0+ earthquake within 50 km during slip or in the subsequent two source durations. Three of the 923 SSEs had an M6.0+ earthquake within three source durations before the SSEs. The relative proportion of large earthquakes following SSEs is insufficient to reject the equal—or unbiased—timing of large earthquakes before or after SSEs. A 95% confidence interval brackets the probability that large earthquakes follow SSEs between 0.3 and 0.9 (using the Klopper-Pearson exact method, and 0.5 is the null hypothesis). Including stress-driven afterslip transients [e.g., (*56*)] would alter these statistics. We conclude that SSEs most commonly occur independently of the nucleation process of large earthquakes.

A more modest contention is that SSEs modulate the earthquake rate and, by extension, drive earthquake swarms (*1*, *18*, *19*, *57*, *58*). The elevated occurrence of earthquakes arising during SSEs is

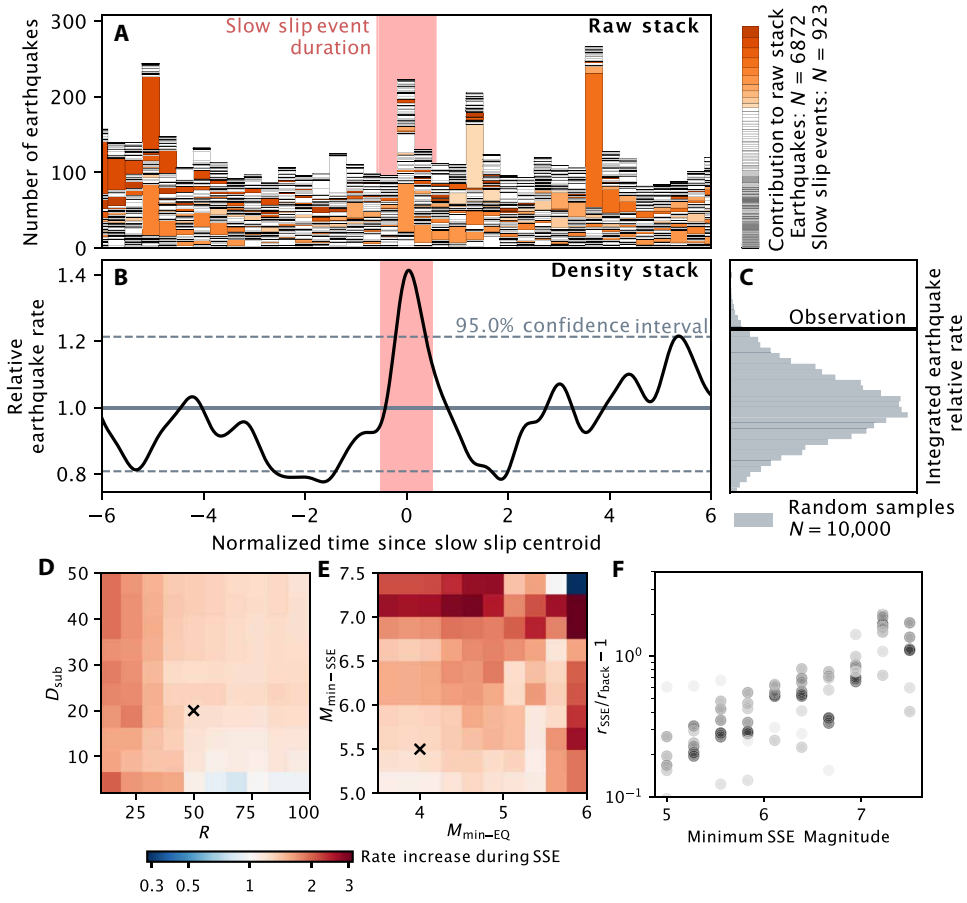

Fig. 3. Seismicity stack. (**A**) Raw seismicity stack. Histogram of earthquake times relative to the centroid time of the corresponding SSEs. Each level represents the contribution from a single SSE's earthquakes. The 10 largest contributors to the raw stack are highlighted in individual shades of orange. (**B**) Stacking densities subdues the effect of earthquake clustering (Eq. 1 in Materials and Methods). The black line represents the relative density stack of earthquake occurrence above a cutoff of M4 within 50 km of the SSE centroids, and ±20 km of the Slab 2.0 geometry (Fig. 1A). (**C**) Comparison of the integrated signal during SSEs for the observed (black) and random (gray) samples. The time-averaged earthquake rate increases to 124 ± 22% of the background. The 95% confidence interval, also shown in (B), is derived from the range in the random samples in (C). (**D** and **E**) Sensitivity of the average rate increases to the maximum epicentral and slab distance (R and D_{sub}, respectively), and the minimum earthquake and SSE magnitude (M_{min-EQ} and $M_{min-SSE}$, respectively). The cross indicates featured parameters (see also table S3). (**F**) Increase in relative earthquake rate as a function of minimum SSE size ($M_{min-SSE}$). The lighter symbols indicate a higher magnitude cutoff for earthquakes (M_{min-EQ}).

unambiguous in the aggregate analysis. However, their overall influence on short-term earthquake probabilities appears to be comparable to prevailing uncertainties and biases in existing forecasting models (*59*). The salient SSE characteristics such as magnitude, depth, and stressing rate are weakly predictive of whether they are abnormally productive (Fig. 5). Nevertheless, their inclusion in forecasting models may contribute to a more comprehensive understanding of seismic activity (*60*).

Slow slip and the mechanics of earthquake triggering

SSEs allow us to probe the nearby faults' response to a stress ramp (Fig. 1A). In the remaining discussion, we touch on additional implications of (i) the amplitude and (ii) the relative timing of the increased earthquake rate related to the occurrence of global SSEs.

Triggering from slow slip versus triggering from earthquakes

The relatively small amplitude of earthquake triggering related to SSEs (Fig. 3 and fig. S9) implies that the moment of an earthquake, whether slow or fast, is an insufficient determinant of its earthquake-triggering potential. The following characteristics set SSEs apart from earthquakes: low stress drop, conditions prone to stable (slow) sliding, and no radiated seismic waves.

SSEs have relatively low slip distributed over a large area, reflecting a stress drop that is in the range of a few kilopascals [e.g., (*31*)], in stark contrast to the 1 to 10 MPa range that is typical for earthquakes [e.g., (*61*)]. However, the influence of stress drop on earthquake triggering is not straightforward. Stress change near the fault is proportional to stress drop on the fault; however, high stress drop also results in a more compact rupture for a given magnitude. Empirically, the effects seem to cancel out for earthquakes—the number of aftershocks is weakly related to stress drop, wherein a high stress drop on a mainshock rupture tends to decrease aftershock productivity (*62*, *63*). For stress drop to be the determinant of an SSE triggering potential, one would need to ascertain why a more distributed low-amplitude stress change is less effective at triggering earthquakes than a more localized high stress change.

One such explanation is that SSEs occur where local conditions are unfavorable to earthquake nucleation. The paucity of earthquakes

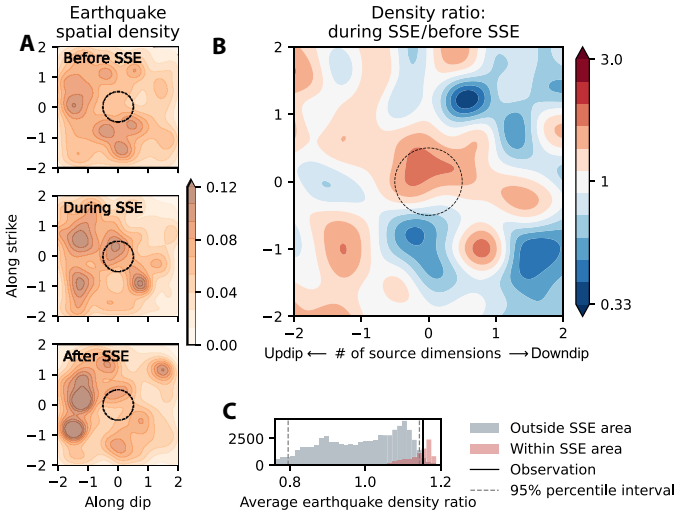

Fig. 4. The influence of slow slip on the spatial distribution of earthquakes. (**A**) Smoothed spatial stacked distribution of earthquakes before (top), during (middle), and after (bottom) all documented SSEs. The timespan before (T_{back}) and after (T_{post}) the SSEs is 6.5 source durations with a 0.5 source duration buffer with respect to the SSE. The periods before and after slow slip display fewer events within the unit source dimension of the SSEs. (**B**) Taking the ratio of the spatial density of earthquakes during the event to the prior window highlights the increase in activity roughly within the limits of the slipping zone (black circle). (**C**) Average earthquake density ratio as measured in the SSE source region is indicated in black. For reference, histograms summarize 10,000 samples with the same footprint size but a random location within ±1.5 source dimensions. The gray histogram and dashed lines comprise the samples that do not overlap with the source dimensions and the corresponding 95% percentile interval; the red histogram comprises samples with origins within the SSE footprint.

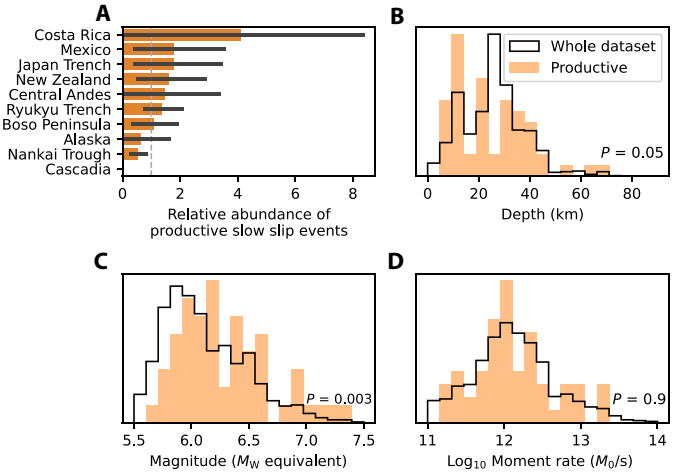

Fig. 5. Examination of the subset of unusually productive SSEs. SSEs are identified as unusually productive if the frequency of comparatively productive random windows in the corresponding background period is less than 5% (see Materials and Methods). (**A**) Relative abundance of productive SSEs. If all regions had an equal proportion of productive SSEs, then they would fall along the dashed line. Error bars indicate the 95% confidence interval on the mean, given 10,000 bootstrap samples from the global set of SSEs. (**B** to **D**) Comparison of source properties (depth, moment magnitude equivalent, and average SSE moment rate) for productive events against the distribution of the global dataset (the *P* value is calculated using the KS test).

triggered by SSEs and, more generally, the complementarity between the distribution of SSEs and earthquakes (*64*) appear to reflect this factor. This reasoning is consistent with fewer background events within the zone of impending slow slip as hinted in the global background seismicity stack (Fig. 4A) and the overall dearth of seismicity in the selected windows (fig. S8). Furthermore, our analysis has neglected explicit consideration of tectonic tremor and associated low-frequency seismic signals, which are frequently observed in tandem with SSEs, appear to illuminate the slow slip process itself, and are generally interpreted to reflect a fluid-rich and high fluid-pressure environment (*65*). Although tremor accounts for a much smaller moment than even modest earthquake triggering (*66*–*68*), the phenomenon is further evidence that conditions near SSEs might be inhibiting earthquake nucleation. It is difficult to distinguish tremorgenic SSEs from nontremorgenic SSEs, with an increasing diversity of observations (*69*); nevertheless, regions canonically associated with tremor, e.g., Nankai and Cascadia, are markedly less prone to feature earthquakes in the dataset. Considering Nankai in isolation, we can see that shallow SSEs are more productive than deep SSEs (fig. S10).

However, an explanation relying solely on the characteristics of the setting also appears incomplete. For illustration, selecting M6+ earthquakes no further than 20 km from the SSE centroids, indicating plausibly overlapping rupture areas, yields a ~300-fold increase above the background rate, following the same stacking procedure (fig. S9). Distributing the rate increase over the median duration of SSEs still yields a ~25-fold increase above the background rate.

Another factor is that earthquake nucleation is sensitive to the characteristics of the transient stressing rate and that the higher dynamic stressing rates associated with earthquakes more effectively drive earthquake nucleation (*70*). Figure 5D suggests that, at least among SSEs, slip rate variations do not result in different earthquake triggering. Weak earthquake triggering around SSEs on the San Andreas Fault, in California, compared to aftershocks of nearby seismic events of similar magnitude has been interpreted as evidence of a major component of dynamic earthquake triggering in typical aftershock sequences (*71*). It is plausible that the lack of ground shaking associated with SSEs contributes to the modest amplitude of observed triggering.

A puzzling implication is that the seismic moment of the triggering event, be it an earthquake or a SSE, is a very incomplete determinant of its triggering potential. If differences between earthquakes and SSEs, as shown in fig. S9, stem from the local susceptibility to earthquake nucleation, those differences must be sufficiently heterogeneous that approximately colocated earthquakes can still generate abundant aftershocks on the megathrust or local faults, while SSEs are not. If the differences stem from differences in radiated energy, then this would imply that dynamic triggering is a much stronger contributor in the near field than previously recognized (*72*).

The timing of triggering from slow slip

The evolution of earthquake rates with respect to the occurrence of an SSE is diagnostic of the underlying trigger mechanism(s) (e.g., Fig. 1). Although observational limitations and stacking obscure details of underlying processes, the resolution of the average time shift between the SSEs and the maximum earthquake rate is increased by stacking. Observations indicate almost no lag (Fig. 3 and figs. S1 and S11), putting in question the mechanisms where SSEs primarily precede or follow earthquakes. Clear preslip episodes (*15*, *17*) or earthquake triggering

of SSEs (*73*, *74*) is a rare occurrence or difficult to resolve (Fig. 1B, i and ii, respectively). According to rate and state frictional models (*75*, *76*), the onset of seismicity is predicted to trail the onset of slow slip (Fig. 1B, iv). Although some of the larger SSEs, those greater than approximately M6.5+, do exhibit a lag (fig. S9), this prediction is inconsistent with the bulk of the observations, unless the relaxation timescale, governed by the earthquake nucleation time and normal stress (*75*), is short relative to the duration of an SSE. Typically, the relaxation timescale is estimated to be on the order of tens of days to a year based on the duration of aftershock sequences (*76*, *77*). Triggering predominantly concurrent with slow slip is consistent with stress loading and yielding during and in the immediate vicinity of SSEs (Fig 1B, iii). An unambiguous diagnostic for the role of fluids is difficult to derive from our observations (Fig 1B, v). Migrating fluids or an equivalent delayed mechanism may be required to explain the range of temporal relationships in the dataset illustrated in the raw temporal stack (Fig. 3A). In summary, the processes enabling the interplay between slow slip and earthquakes have to explain the subdued, concurrent, and highly variable earthquake intensity.

In summary, this study provides a global overview of the interplay between SSEs and earthquakes. We assemble the largest dataset of SSEs to date, with nearly 1000 unique geodetically determined events. Having sufficient statistical power to resolve the influence of slow slip is critical for characterizing the associated earthquake hazard and understanding the underlying mechanisms of slow slip. Global coverage contextualizes the prevalence of unusually seismically productive SSEs indicating that, even when normalizing for the respective low base rates of earthquakes, Nankai and Cascadia are notably less productive than the remaining regions. In the rare cases (9 of 923) where SSEs are associated with larger $M > 6$ earthquakes, the bias for large earthquakes to coincide with or follow, rather than precede, the onset of slow slip is statistically insignificant. A moderate increase in nearby earthquake rates concurrent with slow slip is much more typical. Our observations provide empirical support for earthquake forecasting models that incorporate slow slip, with a base rate that aligns with the geodetic slip rate [e.g., (*19*)]. SSEs not only can document transitional frictional environments that load the megathrust but can also host large earthquakes and vigorous aftershock sequences. The intensity and timing of seismicity associated with SSEs suggest that static stress change alone does not determine earthquake triggering. This comprehensive analysis establishes that while SSEs influence seismicity, their role in directly precipitating moderate or large earthquakes is limited.

MATERIALS AND METHODS

All the scripts and raw data used to recreate the figures in this study are available at https://zenodo.org/records/11095805.

Data

Slow slip events

Catalogs and selection criteria. Our dataset aggregates individual analyses from various regions. See table S1 for a summary. The dataset includes 1204 unique SSE detections from 31 catalogs all using geodetic detection. Enforcing contiguous coverage yields the following focus regions: Mexico, Costa Rica, central Andes, New Zealand, and Japan. Because most of the SSEs in the dataset are in Japan, we opt to further subdivide Japan into the following subregions: Ryukyu, Nankai, Boso, and the Japan trench. All regions feature at least a decade of continuous coverage fig. S1.

The dataset does not include proxy detections derived from tremors, swarms, or repeaters. We also do not consider earthquake afterslip; we refer readers to (*56*) for a comprehensive compilation and analysis thereof. The selection criteria attempt to limit ambiguity in the definition of events and circularity between the abundance of earthquakes and detectability of slow slip.

Imputing missing data. All source properties are not always available in the original reference. In some cases, centroid location and depth, duration, or source dimensions are missing. In these cases, we impute these missing values. When possible, we obtain centroids by digitizing the location of maximum slip; this was done in the case of SSEs in Cascadia and Costa Rica. In the absence of a centroid time, we record the time of maximum slip. As a last resort, if maximum slip is not available, then we use the midpoint time between the start and the end date of the SSE. If depths are not specified, then the centroid depth is obtained by interpolating the Slab 2.0 geometry (*78*) given the centroid latitude and longitude of the SSE. Because we expect very significantly different source dimensions arising from the different processing methods, we derive source dimensions using a shared representative stress drop value (see table S3). In this way, we avoid biasing results because of differences in the determination of source dimensions and use standard earthquake scaling relationships to determine the approximate dimensions. If duration is missing, then we use a scaling relationship derived directly from the data. These approaches to impute the data are coarse; however, as we will see in the following section, the determination of slow slip source properties (and earthquake locations) is subject to substantial uncertainties. The statistical analysis of earthquake rates presented in the main text is designed to be relatively insensitive to measurement uncertainty.

Combining catalogs. For the datasets in Japan, numerous studies provide complementary spatial, temporal, and methodological contributions to the set of regional detection. In the absence of an authoritative dataset for the entire region, it is necessary to combine catalogs and remove duplicate events. We find substantial differences in detections, timing, location, and segmentation. To combine the catalogs, we use a simple windowing approach, wherein all events that are within $R_{\text{duplicate}}$ and $T_{\text{duplicate}}$ from each other are flagged as candidate duplicates (table S2). If the events are from the same reference, then we infer that these are indeed separate events and preserve all detections. When detections issued from different references are flagged as duplicates, we preserve the detection from the more recent publications.

Earthquakes

We consider the SSE detections alongside earthquake catalog data queried using Obspy with the Incorporated Research Institutions for Seismology (IRIS) client (*79*), which in turn queries the International Seismological Center (ISC) Belletin and the National Earthquake Information Center (NEIC) for event data (*49*–*51*, *80*). The global catalog is generally considered complete down to earthquakes around $4.3 \leq \text{Mc} \leq 5.0$, although we expect the subduction zones featured in the analysis to be among the better-instrumented regions and therefore more complete (*81*). We corroborate the following analysis with an exploration of the sensitivity to the magnitude cutoff (Fig. 3). We choose to use the global earthquake catalog, rather than local catalogs, to maintain a uniform and consistent analysis across the different subduction zone settings.

Temporal stacking using Gaussian kernel density estimate

We select all earthquakes above a threshold magnitude M_{min} within a slab-perpendicular distance D_{sub} of the global subduction zone model

geometry (*78*). We assume, as is commonly the case, that the SSEs occur on the plate interface. The earthquakes may be on the slab interface or in the upper or lower plate. For each SSE, we identify a set of earthquakes within a window $\pm T/2$ source durations and R kilometer of the SSE centroid, requiring that there be at least one earthquake in the selected window. We combine each set of earthquakes on a shared timeline measured relative to the centroid time of their corresponding SSEs. We apply a kernel density estimate using a Gaussian kernel with a bandwidth h for a smoothed baseline. To weigh the contribution of each SSE equally, weights are set to the inverse number of earthquakes in each set. This is equivalent to stacking the earthquake temporal densities in each window of observation. T is measured in the number of SSE durations, and therefore, the absolute duration of the observational window varies for each SSE.

The final stacked time series is defined as the double sum over all sets of earthquakes associated with all SSEs

$$f(t') = \frac{1}{M\sqrt{2\pi}} \sum_{j=1}^{M} \sum_{i=1}^{N_j} \frac{1}{N_j} \exp\left(\frac{-(t' - t'_{ij})^2}{2h^2} \right) \quad (1)$$

where $\{t'_{ij};\ i = 1,2, \ldots, N_j\}$ are relative earthquake times and $\{N_j;\ j = 1,2, \ldots, M\}$ are the number of earthquakes associated with the corresponding M SSEs. Here, $t'_{ij} = \left(t_{ij}^{EQ} - t_j^{SSE}\right) / T_j^{SSE}$, where t_{ij}^{EQ} is the earthquake times, t_j^{SSE} is SSE centroid times, and T_j^{SSE} is the corresponding event durations for the j-th SSE. Hence, the time series $f(t')$ is considered with respect to the normalized time since the centroid time of the SSE.

The stacking approach has the following benefits: (i) We stack relative changes in seismicity rather than an absolute change and therefore can compare regions with different base rates of seismicity; (ii) we largely circumvent the need to decluster the earthquake catalogs since the influence of a cluster remains confined to a single window; (iii) we avoid making strong assumptions about the data and the generative model of seismicity; (iv) provided that the magnitude of completeness does not change during the period of observation, we do not expect results to be strongly sensitive to the choice of M_{min}; (v) it does not rely on there being a large number of earthquakes in each window; and (vi) the approach is simple and easy to reproduce. One limitation of the approach, which is not necessarily unique to it, is that windows of observation with no earthquakes do not contribute to the stack. These eventless windows are a fundamentally ambiguous measurement of a relative rate change.

Measuring the amplitude of a rate increase

We can measure the amplitude of the rate increase by comparing the observed distribution of event times against a uniformly distributed set of events. If we measure the amplitude over a fixed interval, for instance, the duration of an SSE, then we compute

$$A = \frac{\int_{T_1}^{T_2} f(t')dt}{\int_{T_1}^{T_2} U(t')dt} = \frac{T}{(T_2 - T_1)} \int_{T_1}^{T_2} f(t')dt \quad (2)$$

Spatial stacking using Gaussian kernel density estimate

Spatial stacking is similar to the temporal stacking approach. The analysis considers all earthquakes within a slab-perpendicular distance D_{sub} of the subduction zone model geometry, and, as a first pass, within 2000 km of the SSE. We then center and reorient the reference frame on the SSE centroids in alignment with the dip direction of the subducting slab geometry. Last, distances are normalized by the dimensions of the SSEs. We use standard scaling relationships for a circular crack assuming a nominal stress drop of $\Delta\sigma_{SSE}$. The inferred source dimensions should not be considered as a precise determination of the spatial extent of the SSEs, but rather as a uniform and self-consistent approach to scaling the dimensions of the analysis. We apply the same weighting and smoothing procedure, now in two dimensions to define maps of seismicity. It is worth noting that we do not report on earthquake rates, but rather on earthquake spatial density, that is, the data are normalized such that they integrate to unity. This treatment captures changes in the structure of the seismicity, but not the abundance in an absolute sense. The background period spans T_{back} and is centered on $t_i^{SSE} - T_{SSE}/2 - T_{buffer} - T_{back}/2$. The slipping period spans T_{SSE} and is centered on each t_i^{SSE}.

Identification of productive SSEs

We test whether the observations reject the null hypothesis that the number of earthquakes measured in the slow slip window might be a random sample from the background period (not containing an SSE), which we estimate empirically (*82*)

$$P_{Null}(N_{co}) \approx \mathbb{E}(N_{co} \geq N_{back}) \quad (3)$$

where we select n random samples with a duration comparable to the average SSE from the background period. Here, P_{Null} is the probability of the null hypothesis, N_{co} is the number of earthquakes in the window of time corresponding to the average SSE duration (co-shocks), and N_{back} is the number of earthquakes during a comparable window of time randomly sampled from the background period. This empirical test obviates the need to decluster the catalog and does not hinge on the assumption that the generative process has some functional form. We expect stable results if the background window is long enough.

This null hypothesis assumes that there are no longer-term variations in the rate of seismicity. For the data we consider, we expect that this assumption may not always hold, particularly in the wake of larger regional earthquakes, where the rate of seismicity steadily decreases as the intensity of the aftershock sequence wanes. Note, however, that this makes this statistical test of significance more stringent because we will always ask whether the last window of time in consideration, expected to have the smallest number of events, has an unusually high number of events. In this way, we expect our test of significance to be conservative. SSEs with $P_{Null}(N_{co}) < 0.05$ are identified as abnormally productive.

Supplementary Materials

This PDF file includes:

Tables S1 to S3
Figs. S1 to S13
References

REFERENCES AND NOTES

1. J.-P. Avouac, From geodetic imaging of seismic and aseismic fault slip to dynamic modeling of the seismic cycle. *Annu. Rev. Earth Planet. Sci.* **43**, 233–271 (2015).

2. R. Bürgmann, The geophysics, geology and mechanics of slow fault slip. *Earth Planet. Sci. Lett.* **495**, 112–134 (2018).
3. R. A. Harris, Large earthquakes and creeping faults. *Rev. Geophys.* **55**, 169–198 (2017).
4. H. Hirose, K. Hirahara, F. Kimata, N. Fujii, S. Miyazaki, A slow thrust slip event following the two 1996 Hyuganada Earthquakes beneath the Bungo Channel, Southwest Japan. *Geophys. Res. Lett.* **26**, 3237–3240 (1999).
5. T. Lay, H. Kanamori, C. J. Ammon, K. D. Koper, A. R. Hutko, L. Ye, H. Yue, T. M. Rushing, Depth-varying rupture properties of subduction zone megathrust faults. *J. Geophys. Res. Solid Earth* **117**, doi.org/10.1029/2011JB009133 (2012).
6. T. Nishimura, Slow slip events in the Kanto and Tokai Regions of Central Japan detected using global navigation satellite system data during 1994–2020. *Geochem. Geophys. Geosyst.* **22**, e2020GC009329 (2021).
7. L. M. Wallace, Slow slip events in New Zealand. *Annu. Rev. Earth Planet. Sci.* **48**, 175–203 (2020).
8. F. Rolandone, J.-M. Nocquet, P. A. Mothes, P. Jarrin, M. Vallée, N. Cubas, S. Hernandez, M. Plain, S. Vaca, Y. Font, Areas prone to slow slip events impede earthquake rupture propagation and promote afterslip. *Sci. Adv.* **4**, eaao6596 (2018).
9. E. E. Brodsky, T. Lay, Recognizing foreshocks from the 1 April 2014 Chile Earthquake. *Science* **344**, 700–702 (2014).
10. V. M. Cruz-Atienza, J. Tago, C. Villafuerte, M. Wei, R. Garza-Girón, L. A. Dominguez, V. Kostoglodov, T. Nishimura, S. I. Franco, J. Real, M. A. Santoyo, Y. Ito, E. Kazachkina, Short-term interaction between silent and devastating earthquakes in Mexico. *Nat. Commun.* **12**, 2171 (2021).
11. Y. Ito, R. Hino, M. Kido, H. Fujimoto, Y. Osada, D. Inazu, Y. Ohta, T. Iinuma, M. Ohzono, S. Miura, M. Mishina, K. Suzuki, T. Tsuji, J. Ashi, Episodic slow slip events in the Japan subduction zone before the 2011 Tohoku-Oki earthquake. *Tectonophysics* **600**, 14–26 (2013).
12. L. Moutote, Y. Itoh, O. Lengliné, Z. Duputel, A. Socquet, Evidence of a Transient Aseismic Slip Driving the 2017 Valparaiso Earthquake Sequence, From Foreshocks to Aftershocks. *J. Geophys. Res. Solid Earth* **128**, e2023JB026603 (2023).
13. M. Radiguet, H. Perfettini, N. Cotte, A. Gualandi, B. Valette, V. Kostoglodov, T. Lhomme, A. Walpersdorf, E. Cabral Cano, M. Campillo, Triggering of the 2014 Mw7.3 Papanoa earthquake by a slow slip event in Guerrero, Mexico. *Nat. Geosci.* **9**, 829–833 (2016).
14. S. Ruiz, M. Metois, A. Fuenzalida, J. Ruiz, F. Leyton, R. Grandin, C. Vigny, R. Madariaga, J. Campos, Intense foreshocks and a slow slip event preceded the 2014 Iquique Mw8.1 earthquake. *Science* **345**, 1165–1169 (2014).
15. C. Cattania, P. Segall, Precursory Slow Slip and Foreshocks on Rough Faults. *J. Geophys. Res. Solid Earth* **126**, e2020JB020430 (2021).
16. G. C. McLaskey, D. A. Lockner, Preslip and cascade processes initiating laboratory stick slip. *J. Geophys. Res. Solid Earth* **119**, 6323–6336 (2014).
17. G. C. McLaskey, B. D. Kilgore, Foreshocks during the nucleation of stick-slip instability. *J. Geophys. Res. Solid Earth* **118**, 2982–2997 (2013).
18. T. Reverso, D. Marsan, A. Helmstetter, B. Enescu, Background seismicity in Boso Peninsula, Japan: Long-term acceleration, and relationship with slow slip events. *Geophys. Res. Lett.* **43**, 5671–5679 (2016).
19. T. Nishikawa, T. Nishimura, Development of an epidemic-type aftershock-sequence model explicitly incorporating the seismicity-triggering effects of slow slip events. *J. Geophys. Res. Solid Earth* **128**, e2023JB026457 (2023).
20. D. Marsan, T. Reverso, A. Helmstetter, B. Enescu, Slow slip and aseismic deformation episodes associated with the subducting Pacific plate offshore Japan, revealed by changes in seismicity. *J. Geophys. Res. Solid Earth* **118**, 4900–4909 (2013).
21. Y. Guo, J. Zhuang, H. Zhang, Detection and characterization of earthquake swarms in Nankai and its association with slow slip events. *J. Geophys. Res. Solid Earth* **128**, e2022JB025984 (2023).
22. S. K. Chen, Y. Wu, Y. Chan, Episodic slow slip events and overlying plate seismicity at the Southernmost Ryukyu Trench. *Geophys. Res. Lett.* **45**, 10369–10377 (2018).
23. Z. El Yousfi, M. Radiguet, B. Rousset, A. Husker, E. Kazachkina, V. Kostoglodov, Intermittence of transient slow slip in the Mexican subduction zone. *Earth Planet. Sci. Lett.* **620**, 118340 (2023).
24. S. Graham, C. DeMets, E. Cabral-Cano, V. Kostoglodov, B. Rousset, A. Walpersdorf, N. Cotte, C. Lasserre, R. McCaffrey, L. Salazar-Tlaczani, "Slow Slip History for the MEXICO Subduction Zone: 2005 Through 2011" in *Geodynamics of the Latin American Pacific Margin*, W. L. Bandy, J. Dañobeitia, C. Gutiérrez, Y. Taran, R. Bartolomé, Eds. (Springer International Publishing, 2017), pp. 3445–3465.
25. S. Itaba, Y. Kitagawa, N. Koizumi, M. Takahashi, N. Matsumoto, N. Takeda, The variation of the strain, tilt and groundwater level in the Shikoku District and Kii Peninsula, Japan (from May to October 2011). *Rep. Coord. Comm. Earthq. Predict.* **87**, 399–418 (2012).
26. S. Itaba, N. Koizumi, M. Takahashi, N. Matsumoto, Y. Kitagawa, T. Ochi, N. Takeda, H. Kimura, T. Kimura, T. Matsuzawa, Short-term slow slip events in the Tokai area, the Kii Peninsula and the Shikoku District, Japan (from May to October 2012). *Rep. Coord. Comm. Earthq. Predict.* **91**, 230–242 (2014).
27. Y. Kitagawa, S. Itaba, N. Koizumi, M. Takahashi, N. Matsumoto, N. Takeda, The variation of the strain, tilt and groundwater level in the Shikoku District and Kii Peninsula, Japan (from November 2010 to May 2011). *Rep. Coord. Comm. Earthq. Predict.* **86**, 519–533 (2011).
28. Y. Kitagawa, S. Itaba, N. Koizumi, M. Takahashi, N. Matsumoto, N. Takeda, H. Kimura, T. Kimura, T. Matsuzawa, K. Shiomi, Short-term slow slip events in the Tokai area, the Kii Peninsula and the Shikoku District, Japan (from November 2011 to April 2012). *Rep. Coord. Comm. Earthq. Predict.* **88**, 303–311 (2012).
29. V. Kostoglodov, S. K. Singh, J. A. Santiago, S. I. Franco, K. M. Larson, A. R. Lowry, R. Bilham, A large silent earthquake in the Guerrero seismic gap, Mexico. *Geophys. Res. Lett.* **30**, doi.org/10.1029/2003GL017219 (2003).
30. A. R. Lowry, K. M. Larson, V. Kostoglodov, R. Bilham, Transient fault slip in Guerrero, southern Mexico. *Geophys. Res. Lett.* **28**, 3753–3756 (2001).
31. S. Michel, A. Gualandi, J.-P. Avouac, Similar scaling laws for earthquakes and Cascadia slow-slip events. *Nature* **574**, 522–526 (2019).
32. T. Nishimura, T. Matsuzawa, K. Obara, Detection of short-term slow slip events along the Nankai Trough, southwest Japan, using GNSS data. *J. Geophys. Res. Solid Earth* **118**, 3112–3125 (2013).
33. T. Nishimura, Short-term slow slip events along the Ryukyu Trench, southwestern Japan, observed by continuous GNSS. *Prog. Earth Planet. Sci.* **1**, 22 (2014).
34. T. Ochi, S. Itaba, N. Koizumi, M. Takahashi, N. Matsumoto, Y. Kitagawa, N. Takeda, H. Kimura, T. Kimura, T. Matsuzawa, Short-term slow slip events in the Tokai area, the Kii Peninsula and the Shikoku District, Japan (from November 2014 to April 2015). *Rep. Coord. Comm. Earthq. Predict.* **94**, 250–261 (2015).
35. Y. Okada, T. Nishimura, T. Tabei, T. Matsushima, H. Hirose, Development of a detection method for short-term slow slip events using GNSS data and its application to the Nankai subduction zone. *Earth Planets Space* **74**, 18 (2022).
36. Y. Okada, T. Nishimura, Systematic detection of short-term slow slip events in southcentral Alaska. *Geophys. Res. Lett.* **50**, e2023GL104901 (2023).
37. B. Rousset, M. Campillo, C. Lasserre, W. B. Frank, N. Cotte, A. Walpersdorf, A. Socquet, V. Kostoglodov, A geodetic matched filter search for slow slip with application to the Mexico subduction zone. *J. Geophys. Res. Solid Earth* **122**, 10498–10514 (2017).
38. S. Sekine, H. Hirose, K. Obara, Along-strike variations in short-term slow slip events in the southwest Japan subduction zone. *J. Geophys. Res. Solid Earth* **115**, (2010).
39. R. Takagi, K. Obara, T. Maeda, Slow slip event within a gap between tremor and locked zones in the Nankai subduction zone. *Geophys. Res. Lett.* **43**, 1066–1074 (2016).
40. R. Takagi, N. Uchida, K. Obara, Along-strike variation and migration of long-term slow slip events in the Western Nankai subduction Zone, Japan. *J. Geophys. Res. Solid Earth* **124**, 3853–3880 (2019).
41. M. Kano, N. Aso, T. Matsuzawa, S. Ide, S. Annoura, R. Arai, S. Baba, M. Bostock, K. Chao, K. Heki, S. Itaba, Y. Ito, N. Kamaya, T. Maeda, J. Maury, M. Nakamura, T. Nishimura, K. Obana, K. Ohta, N. Poiata, B. Rousset, H. Sugioka, R. Takagi, T. Takahashi, A. Takeo, Y. Tu, N. Uchida, Y. Yamashita, K. Obara, Development of a Slow Earthquake Database. *Seismol. Res. Lett.* **89**, 1566–1575 (2018).
42. K. Yano, M. Kano, l_1 trend filtering-based detection of short-term slow slip events: Application to a GNSS array in Southwest Japan. *J. Geophys. Res. Solid Earth* **127**, e2021JB023258 (2022).
43. J. Jara, R. Jolivet, A. Socquet, D. Comte, E. O. Norabuena, Detection of slow slip events along the southern Peru-northern Chile subduction zone. *Authorea Prepr.* 10.22541/essoar.168319853.39124142/v1 , (2023).
44. M. Perry, C. Muller, M. Protti, L. Feng, E. M. Hill, Shallow slow slip events identified offshore the Osa Peninsula in Southern Costa Rica from GNSS time series. *Geophys. Res. Lett.* **50**, e2023GL104771 (2023).
45. M. Radiguet, F. Cotton, M. Vergnolle, M. Campillo, B. Valette, V. Kostoglodov, N. Cotte, Spatial and temporal evolution of a long term slow slip event: the 2006 Guerrero Slow Slip Event. *Geophys. J. Int.* **184**, 816–828 (2011).
46. S. Xie, T. H. Dixon, R. Malservisi, Y. Jiang, M. Protti, C. Muller, Slow Slip and Inter-transient Locking on the Nicoya Megathrust in the Late and Early Stages of an Earthquake Cycle. *J. Geophys. Res. Solid Earth* **125**, e2020JB020503 (2020).
47. L. Marill, D. Marsan, A. Socquet, M. Radiguet, N. Cotte, B. Rousset, Fourteen-year acceleration along the Japan trench. *J. Geophys. Res. Solid Earth* **126**, e2020JB021226 (2021).
48. C. A. Williams, L. M. Wallace, The impact of realistic elastic properties on inversions of shallow subduction interface slow slip events using seafloor geodetic data. *Geophys. Res. Lett.* **45**, 7462–7470 (2018).
49. R. P. Masse, R. E. Needham, NEIC–the National Earthquake Information Center. *Earthq. Volcanoes USGS* **21**, 4–44 (1989).
50. D. A. Storchak, J. Harris, L. Brown, K. Lieser, B. Shumba, D. Di Giacomo, Rebuild of the Bulletin of the International Seismological Centre (ISC)—part 2: 1980–2010. *Geosci. Lett.* **7**, 18 (2020).
51. I. Bondár, D. Storchak, Improved location procedures at the International Seismological Centre. *Geophys. J. Int.* **186**, 1220–1244 (2011).

52. K. Obara, A. Kato, Connecting slow earthquakes to huge earthquakes. *Science* **353**, 253–257 (2016).
53. N. Uchida, T. Iinuma, R. M. Nadeau, R. Bürgmann, R. Hino, Periodic slow slip triggers megathrust zone earthquakes in northeastern Japan. *Science* **351**, 488–492 (2016).
54. G. C. Beroza, W. L. Ellsworth, Properties of the seismic nucleation phase. *Tectonophysics* **261**, 209–227 (1996).
55. J. H. Dieterich, Preseismic fault slip and earthquake prediction. *J. Geophys. Res. Solid Earth* **83**, 3940–3948 (1978).
56. R. M. Churchill, M. J. Werner, J. Biggs, Å. Fagereng, Afterslip moment scaling and variability from a global compilation of estimates. *J. Geophys. Res. Solid Earth* **127**, e2021JB023897 (2022).
57. A. L. Llenos, J. J. McGuire, Detecting aseismic strain transients from seismicity data. *J. Geophys. Res. Solid Earth* **116**, doi.org/10.1029/2010JB007537 (2011).
58. A. L. Llenos, J. J. McGuire, Y. Ogata, Modeling seismic swarms triggered by aseismic transients. *Earth Planet. Sci. Lett.* **281**, 59–69 (2009).
59. S. Seif, A. Mignan, J. Douglas Zechar, M. J. Werner, S. Wiemer, Estimating ETAS: The effects of truncation, missing data, and model assumptions. *J. Geophys. Res. Solid Earth* **122**, 449–469 (2017).
60. T. Jordan, Y.-T. Chen, P. Gasparini, R. Madariaga, I. Main, W. Marzocchi, G. Papadopoulos, K. Yamaoka, J. Zschau, Operational earthquake forecasting: State of knowledge and guidelines for implementation. *Ann. Geophys.* **54**, doi.org/10.4401/ag-5350 (2011).
61. B. P. Allmann, P. M. Shearer, Global variations of stress drop for moderate to large earthquakes. *J. Geophys. Res. Solid Earth* **114**, doi.org/10.1029/2008JB005821 (2009).
62. K. Dascher-Cousineau, E. E. Brodsky, T. Lay, T. H. W. Goebel, What controls variations in aftershock productivity? *J. Geophys. Res. Solid Earth* **125**, 10.1029/2019jb018111 (2020).
63. N. Wetzler, E. E. Brodsky, T. Lay, Regional and stress drop effects on aftershock productivity of large megathrust earthquakes. *Geophys. Res. Lett.* **43**, 12012–12020 (2016).
64. T. Nishikawa, S. Ide, T. Nishimura, A review on slow earthquakes in the Japan Trench. *Prog. Earth Planet Sci.* **10**, 1 (2023).
65. W. M. Behr, R. Bürgmann, What's down there? The structures, materials and environment of deep-seated slow slip and tremor. *Philos. Trans. R. Soc. Math. Phys. Eng. Sci.* **379**, 20200218 (2021).
66. J. Gomberg, A. Wech, K. Creager, K. Obara, D. Agnew, Reconsidering earthquake scaling. *Geophys. Res. Lett.* **43**, 6243–6251 (2016).
67. L. Passarelli, P. A. Selvadurai, E. Rivalta, S. Jónsson, The source scaling and seismic productivity of slow slip transients. *Sci. Adv.* **7**, eabg9718 (2021).
68. G. Rogers, H. Dragert, Episodic tremor and slip on the cascadia subduction zone: The chatter of silent slip. *Science* **300**, 1942–1943 (2003).
69. T. Nishikawa, T. Matsuzawa, K. Ohta, N. Uchida, T. Nishimura, S. Ide, The slow earthquake spectrum in the Japan Trench illuminated by the S-net seafloor observatories. *Science* **365**, 808–813 (2019).
70. E. R. Heimisson, J.-P. Avouac, Analytical prediction of seismicity rate due to tides and other oscillating stresses. *Geophys. Res. Lett.* **47**, e2020GL090827 (2020).
71. F. F. Pollitz, M. J. S. Johnston, Direct test of static stress versus dynamic stress triggering of aftershocks. *Geophys. Res. Lett.* **33**, doi.org/10.1029/2006GL026764 (2006).
72. K. Richards-Dinger, R. S. Stein, S. Toda, Decay of aftershock density with distance does not indicate triggering by dynamic stress. *Nature* **467**, 583–586 (2010).
73. E. Araki, D. M. Saffer, A. J. Kopf, L. M. Wallace, T. Kimura, Y. Machida, S. Ide, E. Davis, Recurring and triggered slow-slip events near the trench at the Nankai Trough subduction megathrust. *Science* **356**, 1157–1160 (2017).
74. T. Taira, R. Bürgmann, R. M. Nadeau, D. S. Dreger, Variability of fault slip behavior along the San Andreas Fault in the San Juan Bautista Region. *J. Geophys. Res. Solid Earth* **119**, 8827–8844 (2014).
75. J. H. Dieterich, A constitutive law for rate of earthquake production and its application to earthquake clustering. *J. Geophys. Res.* **99**, 2601–2618 (1994).
76. P. Segall, E. K. Desmarais, D. Shelly, A. Miklius, P. Cervelli, Earthquakes triggered by silent slip events on Kīlauea volcano, Hawaii. *Nature* **442**, 71–74 (2006).
77. S. Toda, R. S. Stein, Why aftershock duration matters for probabilistic seismic hazard assessment. *Bull. Seismol. Soc. Am.* **108**, 1414–1426 (2018).
78. G. P. Hayes, G. L. Moore, D. E. Portner, M. Hearne, H. Flamme, M. Furtney, G. M. Smoczyk, Slab2, a comprehensive subduction zone geometry model. *Science* **362**, 58–61 (2018).
79. M. Beyreuther, R. Barsch, L. Krischer, T. Megies, Y. Behr, J. Wassermann, ObsPy: A Python Toolbox for Seismology. *Seismol. Res. Lett.* **81**, 530–533 (2010).
80. International Seismological Centre On-line Bulletin; 10.31905/D808B830.
81. J. Woessner, S. Wiemer, Assessing the quality of earthquake catalogues: estimating the magnitude of completeness and its uncertainty. *Bull. Seismol. Soc. Am.* **95**, 684–698 (2005).
82. K. L. Pankow, D. Kilb, Going beyond rate changes as the sole indicator for dynamic triggering of earthquakes. *Sci. Rep.* **10**, 4120 (2020).
83. E. Caballero, A. Chounet, Z. Duputel, J. Jara, C. Twardzik, R. Jolivet, Seismic and aseismic fault slip during the initiation phase of the 2017 MW = 6.9 valparaíso earthquake. *Geophys. Res. Lett.* **48**, e2020GL091916 (2021).
84. R. B. Lohman, J. J. McGuire, Earthquake swarms driven by aseismic creep in the Salton Trough, California. *J. Geophys. Res. Solid Earth* **112**, (2007).
85. M. Vallee, J.-M. Nocquet, J. Battaglia, Y. Font, M. Segovia, M. Regnier, P. Mothes, P. Jarrin, D. Cisneros, S. Vaca, M. Vallée, M. Segovia, M. Régnier, P. Jarrin, D. Cisneros, S. Vaca, H. Yepes, X. Martin, N. Béthoux, M. Chlieh, Intense interface seismicity triggered by a shallow slow slip event in the Central Ecuador subduction zone. *J. Geophys. Res. Solid Earth* **118**, 2965–2981 (2013).
86. K. Sirorattanakul, Z. E. Ross, M. Khoshmanesh, E. S. Cochran, M. Acosta, J.-P. Avouac, The 2020 Westmorland, California Earthquake Swarm as Aftershocks of a Slow Slip Event Sustained by Fluid Flow. *J. Geophys. Res. Solid Earth* **127**, e2022JB024693 (2022).
87. E. Warren-Smith, B. Fry, L. Wallace, E. Chon, S. Henrys, A. Sheehan, K. Mochizuki, S. Schwartz, S. Webb, S. Lebedev, Episodic stress and fluid pressure cycling in subducting oceanic crust during slow slip. *Nat. Geosci.* **12**, 475–481 (2019).
88. A. C. Gase, N. L. Bangs, D. M. Saffer, S. Han, P. K. Miller, R. E. Bell, R. Arai, S. A. Henrys, S. Kodaira, R. Davy, L. Frahm, D. H. N. Barker, Subducting volcaniclastic-rich upper crust supplies fluids for shallow megathrust and slow slip. *Sci. Adv.* **9**, eadh0150 (2023).
89. J. Nakajima, N. Uchida, Repeated drainage from megathrusts during episodic slow slip. *Nat. Geosci.* **11**, 351–356 (2018).
90. S. Itaba, N. Koizumi, M. Takahashi, N. Matsumoto, Y. Kitagawa, T. Ochi, N. Takeda, H. Kimura, T. Kimura, T. Matsuzawa, Short-term slow slip events in the Tokai area, the Kii Peninsula and the Shikoku District, Japan (from May to October 2012). *Rep. Coord. Comm. Earthq. Predict.* **93**, 330–335 (2015).
91. S. Michel, A. Gualandi, J.-P. Avouac, Interseismic coupling and slow slip events on the cascadia megathrust. *Pure Appl. Geophys.* **176**, 3867–3891 (2019).
92. H. Gao, D. A. Schmidt, R. J. Weldon II, Scaling relationships of source parameters for slow slip events. *Bull. Seismol. Soc. Am.* **102**, 352–360 (2012).
93. Y. Shi, B. A. Bolt, The standard error of the magnitude-frequency *b*-value. *Bull. Seismol. Soc. Am.* **72**, 1677–1687 (1982).

Acknowledgments: We thank the members of the BSL, J. Ojeda, S. Schwartz, and A. Rodriguez Padilla for providing thoughtful insight and discussion. **Funding:** K.D.-C. received support from the Miller Institute for basic science. R.B. acknowledges funding by NSF award EAR-2028554. **Author contributions:** Conceptualization: K.D.-C. and R.B. Data curation: K.D.-C. Formal analysis: K.D.-C. Methodology: K.D.-C. and R.B. Investigation: K.D.-C. and R.B. Visualization: K.D.-C. Funding acquisition: K.D.-C. Supervision: R.B. Writing—original draft: K.D.-C. and R.B. Writing—review and editing: K.D.-C. and R.B. **Competing interests:** The authors declare that they have no competing interests. **Data and materials availability:** All data needed to evaluate the conclusions in the paper are present in the paper and/or the Supplementary Materials. Code used to produce figures, along datasets and example workflows are available at https://zenodo.org/records/11095805. We queried earthquake catalogs from the using the IRIS DMC FDSNWS event Web Services, which in turn queries the ISC catalog (https://doi.org/10.31905/D808B830) and the NEIC catalogs (https://earthquake.usgs.gov/earthquakes/search/). A full global catalog of SSEs as prepared for this study is available for download in the Supplementary Materials. A major portion of the catalogs were available through the slow earthquake database (www-solid.eps.s.u-tokyo.ac.jp/~sloweq/).

Submitted 24 January 2024
Accepted 25 July 2024
Published 30 August 2024
10.1126/sciadv.ado2191